NANO · MICRO small
www.small-journal.com

Hyperboloid-Drum Microdisk Laser Biosensors for Ultrasensitive Detection of Human IgG

Zhihe Guo, Yingchun Qin, Peizong Chen, Jinliang Hu, Yi Zhou, Xuyang Zhao, Zhiran Liu, Yiyan Fei, Xiaoshun Jiang, and Xiang Wu**

Whispering gallery mode (WGM) microresonators have been used as optical sensors in fundamental research and practical applications. The majority of WGM sensors are passive resonators that require complex systems, thereby limiting their practicality. Active resonators enable the remote excitation and collection of WGM-modulated fluorescence spectra, without requiring complex systems, and can be used as alternatives to passive microresonators. This paper demonstrates an active microresonator, which is a microdisk laser in a hyperboloid-drum (HD) shape. The HD microdisk lasers are a combination of a rhodamine B-doped photoresist and a silica microdisk. These HD microdisk lasers can be utilized for the detection of label-free biomolecules. The biomolecule concentration can be as low as 1 ag mL^{-1}, whereas the theoretical detection limit of the biosensor for human IgG in phosphate buffer saline is 9 ag mL^{-1} (0.06 a_M). Additionally, the biosensors are able to detect biomolecules in an artificial serum, with a theoretical detection limit of 9 ag mL^{-1} (0.06 a_M). These results are approximately four orders of magnitude more sensitive than those for the typical active WGM biosensors. The proposed HD microdisk laser biosensors show enormous detection potential for biomarkers in protein secretions or body fluids.

1. Introduction

Owing to their high quality (Q) factors and small mode volumes, whispering gallery mode (WGM) resonators have been utilized in a wide variety of fundamental research and practical applications in recent years.[1–6] Significant progress has been made in the development of optical microcavity technology for biological detection and recent research activity has been focused mainly on the development of high sensitivity detection schemes.[7–10] WGM biosensors present a noninvasive technique for real-time investigations and label-free detection of biomolecules.[11] Due to the improvements in fabrication and detection methods, some WGM biosensors, such as those utilizing microtoroid and microbubble resonators, have the ability to detect biomolecules down to concentrations of several a_M or fg mL^{-1}.[12,13] Microbead biosensors have achieved the real-time detection of biomarkers (cytochrome c) released from cells, and have a detection limit of 6.82 p_M.[14] However, most WGM biosensors are passive devices, which require evanescent-wave couplers such as waveguides or fiber tapers to achieve the excitations of the WGMs.[15–17] The coupling position between the microcavity and the evanescent-wave coupler is easily influenced by various external perturbations, which can greatly affect the reliability of the experimental results.[18,19] Although some effective methods have been applied to eliminate these disturbances and improve the stability of the biosensors, such as the locked frequency method, thermal control method, whole packaged method, and external reference method,[13,14,20–22] they typically increase the complexity and cost, which limits the practicality of the biosensors.

Active WGM resonators, which typically contain a fluorescent or gain medium, are particularly suitable for the simultaneous remote excitation, probing, and collection of the WGM signal.[23,24] These active resonators alleviate some of the practical limitations of typical passive WGM resonators, allowing their use in a number of applications; the same is not possible when using passive resonators. However, because fluorescence-based WGM biosensors have considerably low Q factors and high detection limits, it is still quite challenging to detect a low concentration of biomolecules using fluorescent biosensors.[15]

Z. H. Guo, J. L. Hu, Y. Zhou, X. Y. Zhao, Z. R. Liu, Prof. Y. Y. Fei, Prof. X. Wu
Key Laboratory of Micro and Nano Photonic Structures (Ministry of Education)
Department of Optical Science and Engineering
Shanghai Engineering Research Center of Ultra Precision Optical Manufacturing
Fudan University
Shanghai 200433, China
E-mail: wuxiang@fudan.edu.cn

Y. C. Qin, Prof. X. S. Jiang
National Laboratory of Solid State Microstructures and College of Engineering and Applied Sciences
Nanjing University
Nanjing 210093, China
E-mail: jxs@nju.edu.cn

P. Z. Chen
State Key Laboratory of Surface Physics and Department of Physics
Fudan University
Shanghai 200433, China

The ORCID identification number(s) for the author(s) of this article can be found under https://doi.org/10.1002/smll.202000239.

DOI: 10.1002/smll.202000239

Lasing-based biosensors have several advantages over their fluorescent counterparts, especially in terms of the high light intensity, narrow mode linewidth, and threshold behavior.[25,26] Additionally, lasing-based biosensors are able to improve the sensing accuracy, compared to fluorescent biosensors.[27,28] On-chip lasing-based resonators are particularly suited for device integration to achieve a compact sensing platform.[23,29] Recently, significant progress has been made with regard to lasing-based WGM biosensors, with their detection limits being improved from several hundred ng mL^{-1} to several dozen pg mL^{-1} (reaching even several dozen p_M).[21,26,30,31] However, many lasing-based WGM biosensors are fabricated from polymers via ultraviolet lithography and development, thereby affecting the surface roughness of the microcavity, making it difficult to obtain a higher *Q*-factor and stronger light–matter interaction, and influencing the sensitivity.[32–36]

In this paper, an ultrasensitive active WGM microresonator, a hyperboloid-drum (HD) microdisk laser, is proposed to detect biomolecules, such as bovine serum albumin (BSA) and human immunoglobulin G (IgG). The HD microdisk laser is fabricated from a silica microdisk coated with the gain medium (rhodamine B-doped photoresist). The WGMs exist in the HD region and the laser light is emitted from the wedge. This type of HD microdisk laser has a *Q* factor on the order of magnitude of 10^5 and a low laser threshold at several μJ mm^{-2}, which can reduce the thermal and dye bleaching effects. After combining with the microfluidic channels, the HD microdisk lasers are utilized for biomolecular detection in aqueous media. The HD microdisk lasers present responses to BSA at concentrations ranging from 1 ag mL^{-1} to 100 ng mL^{-1}, and to human IgG at concentrations ranging from 1 ag mL^{-1} to 100 μg mL^{-1}. This means that the biosensors can respond to a slight change of the biomolecule concentration.

2. Results and Discussion

2.1. Optical Characteristics

The scanning electron microscopy (SEM) images of the silica microdisks and HD microdisk-lasers are shown in **Figure 1**a–d, respectively. These HD microdisk lasers are a combination of a rhodamine B-doped photoresist (SU-8) and a silica microdisk. The HD shape is formed as an effect of the surface tension after the spin-coating process. The wedge angle of the HD region is ≈30°; the thickness of the HD microdisk laser, labeled as h_1, is 1.9 μm and the height of the HD microdisk laser, labeled as h_2, is 12.5 μm; all measurements were made by SEM, as shown in Figure 1d.

Figure 2a shows the schematic diagram of the HD microdisk laser. The spectrum of the HD microdisk laser in water is plotted in Figure 2b. Using a Lorentzian fitting to estimate the WGM of the microdisk laser, the full-width at half-maximum of the lasing peak at 639.803 nm is ≈0.027 nm, which is limited by the spectrometer's spectral resolution (≈0.015 nm). The free spectral range (FSR) obtained from this spectrum is 1.619 nm, which agrees well with the theoretically estimated FSR of 1.612 nm. The passive resonances of the HD microdisk were scanned with a tunable laser (≈780 nm) and the *Q* factor

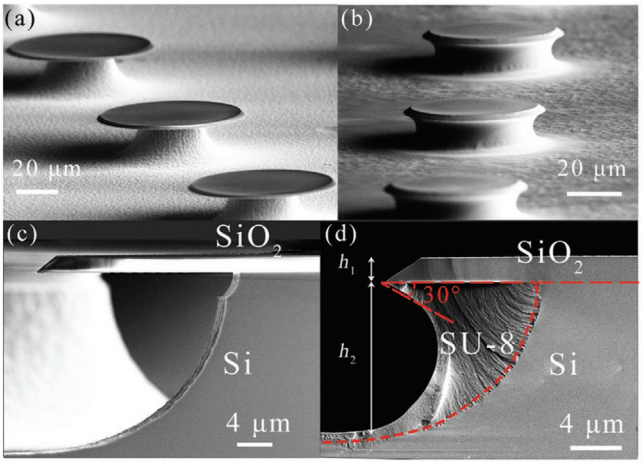

Figure 1. a,b) SEM images of blank microdisks and HD microdisk lasers, respectively. c,d) Cross-section views of the SEM images of a blank silica microdisk and an HD microdisk laser, respectively. The angle of the wedge in the HD region (SU-8) in (d) is ≈30°. h_1 is 1.9 μm and h_2 is 12.5 μm.

of the HD microdisk is ≈1.0×10^5, as shown in the insert of Figure 2b. In Figure 2c, the lasing characteristics obtained by exciting an HD microdisk immersed in water with different excitation energy densities are presented. The lasing threshold of the HD microdisk laser is ≈8.40 μJ mm^{-2}. The high *Q* value decreases the pumping laser power, reduces the thermal effects, and reduces the dye bleaching effects. The active layer on the SiO_2 microdisk surface is not sufficiently thick enough to form a good confinement of the WGMs. Therefore, the laser mode field is only generated and distributed within the wedge region (rhodamine B-doped photoresist). The numerical simulation results based on the finite element method (FEM) are shown in Figure 2d and Figure S1 (Supporting Information).

2.2. Measurement of Bulk Refractive Index Sensitivity

To facilitate subsequent experiments, the wavelength stability of the HD microdisk laser was measured in water. The wavelength shift of the laser as a function of time was measured over a 2000 s interval, as shown in **Figure 3**a. The central wavelengths of the laser peaks were obtained by Lorentz fitting and are plotted in Figure 3b. The standard deviation (SD) of this curve is 3.98 pm. The slight blue shift of the wavelength is caused by the bleaching of the rhodamine B dye. These results indicate that the stability of the HD microdisk laser is sufficient for subsequent experiments.

The measurement of the bulk refractive index sensitivity (*S*) was characterized by introducing aqueous solutions with different refractive indices. Each solution was extracted into or out of the microfluidic channels independently by using a syringe pump as shown in Figure S2 (Supporting Information). When different concentrations of the dimethyl sulfoxide (DMSO) solutions were extracted into the microfluidic channel, it caused the WGM position to shift to a longer wavelength. The refractive indices of the DMSO solutions are proportional to the volume ratios of the DMSO and can be calculated using the mixing rules.[37] The experimental sensitivity (S_{Exp}) of the HD microdisk

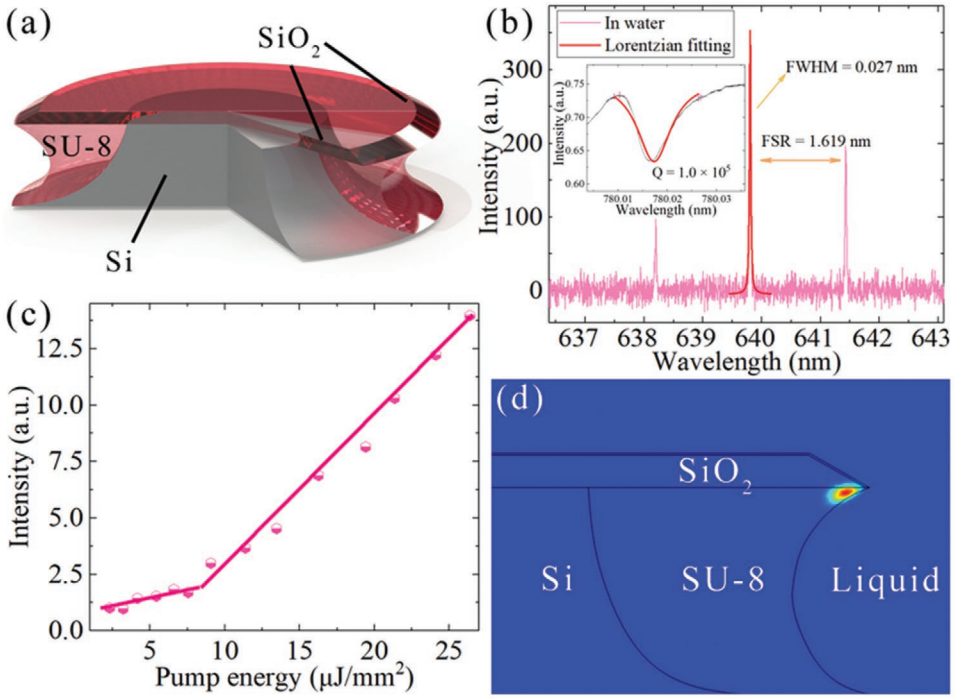

Figure 2. Optical characteristics of HD microdisk lasers. a) Schematic drawing of an HD microdisk laser. b) Spectra of the HD microdisk laser immersed in water. Full-width at half-maximum of the lasing peak was estimated to be 0.027 nm. FSR is 1.619 nm. Insert: Transmission spectrum of HD microdisk lasers detected under a tunable laser (central wavelength is 780 nm). The Q factor is ≈1.0×10^5. c) Output laser intensity versus pump laser energy of HD microdisk laser immersed in water at room temperature. d) Field distribution of WGM in fundamental-order-radial mode at 648.28 nm. Refractive index of the liquid was set as $n = 1.33$.

laser is 18.2 nm RIU^{-1}, as shown in Figure 3c,d. Using the FEM to simulate the S of the microdisk laser, the simulated sensitivity (S_{Sim}) of the first-order radial WGM mode is 18.4 nm RIU^{-1}, which agrees well with the experimental results.

The relation between the S and the fraction of the light energy in the liquid (η) is[38]

$$S = \frac{\delta\lambda}{\delta n} \approx \frac{\lambda}{n_1}\eta \tag{1}$$

where δn is the refractive index change of the liquid; n_1 is the refractive index of the microcavity; and $\delta\lambda$ is the wavelength shift in resonant wavelength (λ). The η can be expressed as[38,39]

$$\eta \cong \frac{n^2 \lambda R h |E_0|^2}{2\varepsilon_{rs}\sqrt{n_1^2 - n^2}\int |E|^2 \, dV} \tag{2}$$

where n is the refractive index of the liquid; R is the radius of the microcavity; h is an arbitrary length along the resonator longitudinal direction; $\epsilon_s = \epsilon_0\epsilon_{rs}$ is the dielectric constant of the resonator; E_0 and E are the electric field in the liquid and the whole space, respectively. The integral in the denominator of Equation (2) is taken over the volume (V) of the whole space. Equation (2) indicates that η is linearly proportional to the light energy in the liquid. Increasing of the electric field in the liquid (E_0) can obtain the greater η and S.

The FEM simulation was used to investigate the influence of the wedge angle on the first-order radial WGM of the microcavity. The η and simulated sensitivity (S_{Sim}) decrease gradually as the wedge angles increase, as shown in Figure 3e,f, respectively. A decreasing in η indicates that the mode field of the HD microdisk laser has been gradually distributed to the inner portion of microcavity, which reduces the interaction intensity between light and matter. The field distributions of the first-order-radial WGM, with different wedge angles, are shown in Figure S1 (Supporting Information). These results suggest that HD microdisks with a smaller wedge are able to achieve a greater η, enhance the interaction between light and matter, which can aid in achieving a higher sensitivity.

2.3. No-Specific Detection of BSA

The biofunctionalization is performed on the silica surface of the HD microdisk-laser, and the sensing procedures are illustrated in **Figure 4**a–c. First, the surfaces of the HD microdisk laser were activated by applying an oxygen plasma for 2 min.[40] Immediately afterward, the microdisk was immersed in an alcohol solution containing 1% 3-glycidoxypropyltrimethoxysilan (GOPTS) to achieve surface silanization, as shown in Figure 4b.[13,41] The HD microdisk laser biosensor was used in the nonspecific detection of BSA (66 kDa). In following experiments, the procedures of the biomolecular detection can refer to the Supporting Information (unless otherwise noted).

The binding of the BSA molecules to the surface of the microdisk laser causes a redshift of the WGM, as shown in Figure 4d,e. In Figure 4e, the wavelength shifts gradually as

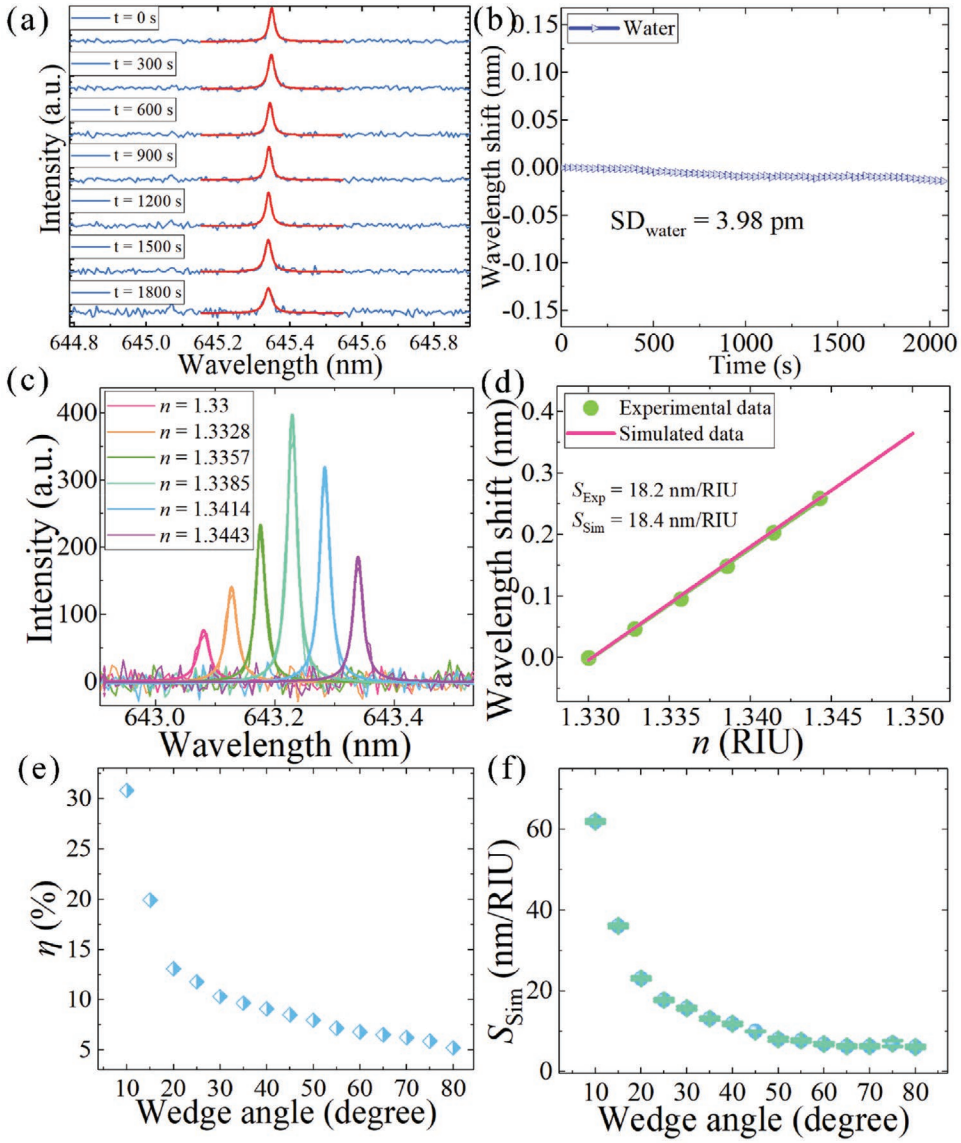

Figure 3. Stability measurement and refractive index sensing of HD microdisk lasers. a) Spectra of HD microdisk laser under different times in water. Blue curves are the experimental data and the red curves are results of Lorentz fittings. b) Wavelength shifts of the laser peaks varies with time in water. Standard deviation (SD_{water}) is 3.98 pm. c) Spectra of laser peaks as a function of different refractive indices. d) Wavelength shifts as a function of refractive index. Green dots are the experimental results and red line is the simulated results. e) η and f) S_{Sim} as a function of wedge angles.

the BSA concentrations are increased due to the enhanced dielectric constant after the BSA has bound to the GOPTS. The vertical coordinate on the right-hand side of Figure 4e is the calculated result of the theoretical molecular surface density (MSD), which is derived from the linear relationship between the wavelength shift of the WGM and the adsorption density of biomolecules on the surface of the HD microdisk laser.[38,39,42] The MSD (σ_s) can be expressed as[42]

$$\sigma_s \cong \frac{\delta\lambda}{\lambda}\frac{\varepsilon_s}{\alpha_{ex}}\frac{R[J_{l+1}^2(k_0nR)]}{[J_l^2(k_0nR)]} \quad (3)$$

where α_{ex} is the excess polarizability of the particles binding to the resonator surface; k_0 represents the wavelength number; J_l is the Bessel function of first kind of order l. The derivations and the parameters of Equation (3) can be found in the Supporting Information.

The BSA binding reached a relatively saturated concentration at 10 pg mL^{-1}; and the measured concentration was as low as 1 ag mL^{-1} (1.5×10^{-20} M). Each error bar represents the SD of three independent measurements. The accumulated wavelength shifts of the biosensors and MSD associated with different concentrations of BSA were fit using a Hill model (R^2 = 0.997).[21] The sensitivity of the linear region was S_{BSA} = 0.010 nm mL ag^{-1}. We use the spectrometer's spectral resolution as the SD of the three-sigma method, where σ = 0.015 nm. The theoretical detection limit (DL) can be estimated as $DL_{BSA} = 3\sigma/S_{BSA}$ = 4.5 ag mL^{-1} (0.068 a$_M$).

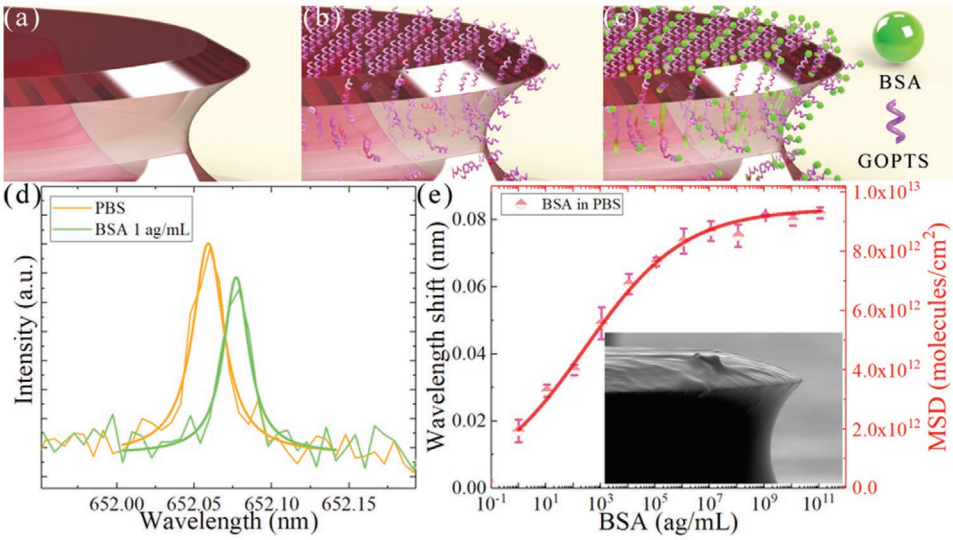

Figure 4. No-specific binding of BSA to the HD microdisk laser surfaces. a–c) Surface activation and sensing processes for BSA binding to the surface of the HD microdisk laser. d) Spectra of the HD microdisk lasers at different BSA concentrations in PBS. e) Wavelength shift and MSD corresponding to the BSA concentrations. Data are fitted by the red curve is the data fitted by Hill model ($R^2 = 0.997$).

2.4. Specific Detection of Human Immunoglobulin G

The ability to detect specific biomarkers is a vital portion of the assessment of health, disease, or vaccination status in modern medical diagnostics.[40] Human IgG (150 kDa) is the main type of antibody found in the blood and extracellular fluid, protecting the body from bacterial and viral infections.[43] Here, HD microdisk-laser biosensors were used to specifically detect human IgG. The surface activation and functionalization procedures are plotted in **Figure 5**a–d. The specific detection was based on the specific binding relationship between goat anti-human IgG and human IgG. Figure 5c shows a representation of goat anti-human IgG (0.1 mg mL^{-1}) being introduced into the microfluidic channel and incubated for half an hour. The goat anti-human IgG then binds to the GOPTS and can be used as a probe to capture the analyte (human IgG). After replacing the goat anti-human IgG and rinsing with phosphate-buffered saline (PBS), BSA (0.1 mg mL^{-1}) was introduced to block the unbound sites, which reduces the probability of nonspecific binding of the analyte (Figure 5d). Half an hour later, the microdisk lasers were rinsed with PBS to remove the residual BSA solution.

Figure 5e shows a representation of the sensing procedure for human IgG. The binding of the human IgG molecules causes a redshift of the WGM, as shown in Figure 5f. Figure 5g presents the relationship between the wavelength shift and MSD and the concentrations of human IgG in PBS, which was fit using a Hill model ($R^2 = 0.995$). The binding process reached a relatively saturated concentration at 10 ng mL^{-1}, and the measured concentration was as low as 1 ag mL^{-1} (6.67×10^{-21} M). Each error bar comes from the SD from three independent measurements of the human IgG. The sensitivity of the linear variation region is $S_{IgG\text{-}1} = 0.005$ nm mL ag^{-1}, and the theoretical DL can be estimated as $DL_{IgG\text{-}1} = 3\sigma/S_{IgG\text{-}1} = 9$ ag mL^{-1} (0.060 a_M). The combinations of the GOPTS and BSA are accomplished through amine-based binding. Additionally, many of the free amine groups covered on the surface of the BSA molecules can quickly bind to the GOPTS.[13] While the absorption of the human IgG and goat anti-human IgG was facilitated through specific binding sites, and is a relatively slow and time-consuming process. Hence, the responses of the BSA bindings are significantly quicker than that of human IgG.

The measured responses to the control proteins served as negative control experiments, in comparison to the target analyte, human IgG, the results are presented in Figure 5h. The concentrations of the tested samples, such as BSA, human IgA, horse IgG, and human IgG solutions, were set to 1 ag mL^{-1}, 1 fg mL^{-1}, 1 pg mL^{-1}, 1 ng mL^{-1}, and 10 µg mL^{-1} in PBS, respectively. The wavelength shifts caused by flowing the BSA, human IgA, and horse IgG solutions were much smaller than those caused by human IgG, when using the same concentration. The stronger wavelength shift caused by the human IgG suggests a good specificity of the biosensor for biomolecular detection.

Numerous previous studies have reported the detections of the biomolecules diluted in PBS.[44–46] However, if the biosensors are able to detect target biomolecules in complex and realistic environments directly, such as in human serum or urine, they would be much more applicable in diagnostics.[47] Therefore, we demonstrated the feasibility of using HD microdisk lasers for detecting biomolecules in an artificial serum. The functionalization and sensing procedures of the HD microdisk-laser are presented in Figure 5a–e. After a stable detection baseline in the PBS environment was established, the PBS was replaced with the artificial serum. The insert in Figure 5i indicates a wavelength shift of 0.062 nm when the solution was changed from the PBS to the artificial serum, with an SD of 2.81 pm for the pink curve. These results indicate that the components in the artificial serum do not affect the surface of the biosensors after functionalization. After this, the specific detection of human IgG in an artificial serum was conducted. Figure 5i shows the relationships between the wavelength shift and MSD and the concentrations of the human IgG in the artificial serum, which was fit using a Hill model ($R^2 = 0.905$). The binding of human IgG

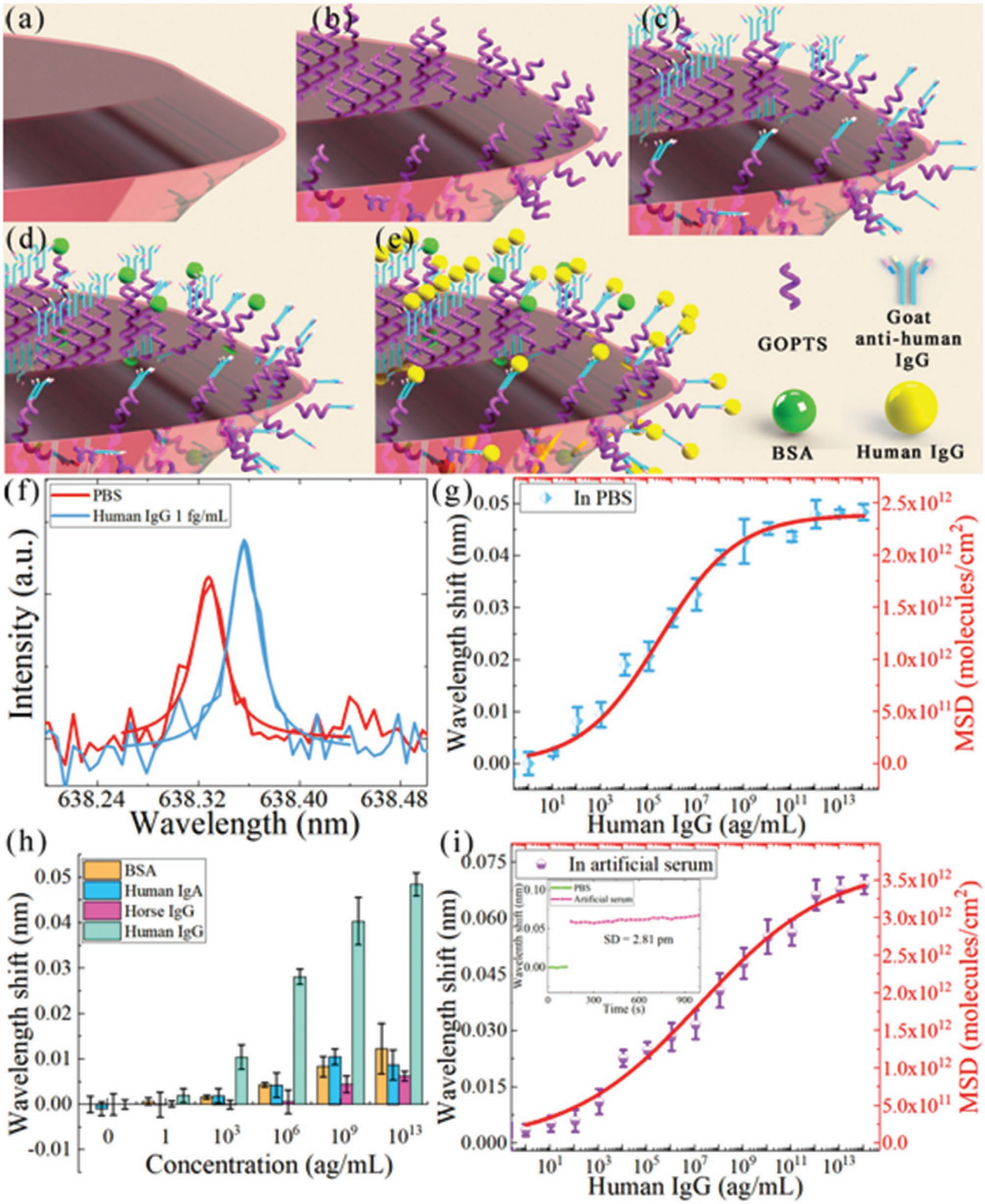

Figure 5. Specific binding of human IgG to the HD microdisk surfaces. a–e) Procedures for detecting human IgG. f) Spectra of the HD microdisk lasers at different concentrations of human IgG in PBS. g) Wavelength shift and MSD corresponding to the concentrations of human IgG in PBS. Data are fitted by the red curve obtained from the Hill model ($R^2 = 0.995$). h) Wavelength shifts response to different control proteins, comparing the target analyte human IgG. i) Wavelength shifts and MSD as a function of human IgG concentrations. Red curve obtained from Hill model fitting of the data ($R^2 = 0.905$). Insert: Wavelength shift caused by PBS solution changing to artificial serum is 0.062 nm. SD is 2.81 pm.

Table 1. Comparison of HD microdisk laser and other optical sensors recently demonstrated for biomolecular detections.

Platform	Type	Analyte	Measure range	Detection limit	Refs.
Optofluidic waveguide	Passive	P-53 protein	10 [fg mL^{-1}]–10 [ng mL^{-1}]	4 [fg mL^{-1}]	[47]
Microtoroid	Passive WGM	Human chorionic gonadotropin	100 [a_M]–10 [n_M]	120 [a_M]	[12]
Microbubble	Passive WGM	D-biotin	4.1 [f_M]–410 [p_M]	4.1 [f_M]	[13]
Microring	Passive WGM	RhS100A4 protein	3 [n_M]–3000 [n_M]	3 [n_M]	[48]
Microring	Passive WGM	Single-stranded DNA	1.95 [n_M]–1 [μ_M]	195 [f_M]	[49]
Microring	Passive WGM	Streptococcus pneumoniae tmRNA	52.4 [f_M]–16.6 [p_M]	53 [f_M]	[50]
Microring	Passive WGM	C-reactive protein	100 [pg mL^{-1}]–10 [μg mL^{-1}]	200 [f_M]	[51]
Microsphere	WGM-nanoshell hybrid	Thyroglobulin	1 [ag]	–	[52]
Microsphere	WGM-nanoshell hybrid	BSA	0.11 [ag]	0.008 [ag]	[52]
Microbubble	Fluorescence	Anti-rabbit IgG	100 [pg mL^{-1}]–100 [μg mL^{-1}]	15 [ng mL^{-1}]	[53]
Aptamer-based biosensor	Fluorescence	Let-7a	10 [a_M]–1 [p_M]	10 [a_M]	[54]
DNA silver metallization	SERS	DNA	100 [p_M]–1 [μ_M]	34 [p_M]	[55]
Microdisk	Active WGM	Streptavidin	1.5 [μg mL^{-1}]	104 [ng mL^{-1}]	[21]
Microgoblet	Active WGM	Streptavidin	1.56 [μg mL^{-1}]–30 [μg mL^{-1}]	352 [ng mL^{-1}]	[56]
Hollow optical fiber	Active WGM	IgG	0 [n_M]–1200 [n_M]	11 [n_M]	[57]
Microsphere	Active WGM	Neutravidin	5 [n_M]–400 [n_M]	25 [n_M]	[22]
HD microdisk	Active WGM	Human IgG	0.007 [a_M]–0.667 [m_M]	0.06 [a_M]	This work

reached a relatively saturated concentration at 1 μg mL^{-1}, and the measured concentration was as low as 1 ag mL^{-1} (6.67×10^{-21} M). The results were similar to the specific detection of human IgG in PBS. Each error bar represents the SD from three independent measurements of the human IgG. The sensitivity of the linear variation region in this case is $S_{IgG\text{-}2} = 0.005$ nm mL ag^{-1}, and the theoretical DL is estimated to be $DL_{IgG\text{-}2} = 3\sigma/S_{IgG\text{-}2} = 9$ ag mL^{-1} (0.060 a_M). These results indicate that the HD microdisk lasers biosensors are able to detect biomolecules diluted not only in PBS but also in an artificial serum, thereby simulating the conditions in human body fluids.

Table 1 presents a series of different types of biomolecule sensing methods that have been reported in recent years.[12,13,21,22,47–57] Compared to the majority of existing optical biosensors, the proposed method, using an HD microdisk laser, has a wider linear sensing region and a much lower DL for biomolecular detections. Previous studies have mentioned that a protein A or protein G binding method was used to maintain the biological activity and orientation of antibodies on the sensor surface.[58] The application of this method considerably increases the binding of human IgG to the goat anti-human IgG and improves the sensitivity of the biosensor. In the next study, we plan on attempting to add the protein A or protein G binding method to further improve the DL of our biosensors.

3. Conclusion

In this paper, a novel HD microdisk laser fabricated from a silica microdisk coated with a gain medium is proposed. WGMs exist only in the HD region of the microdisk and the laser is emitted from the wedge. The HD microdisk laser has a Q factor on the order of magnitude of 10^5 and a low laser threshold, at several μJ mm^{-2}. The HD microdisk-laser biosensors are responsive to BSA at concentrations ranging from 1 ag mL^{-1} to 100 ng mL^{-1}, and to human IgG at concentrations ranging from 1 ag mL^{-1} to 100 μg mL^{-1}. The nonspecific detection limit for BSA in PBS is 4.5 ag mL^{-1} (0.068 a_M); for human IgG in PBS and artificial serum, the specific detection limits are both 9 ag mL^{-1} (0.060 a_M). The ultralow detection limits in biomolecular detections show the biosensing capabilities of the HD microdisk laser. The proposed HD microdisk laser represents a promising prospect in the realization of a high-throughput channel biosensor for in vitro detections in protein secretions or body fluids.

4. Experimental Section

Materials and Reagents Preparations: The photoresist used was the SU-8 (SU-8 2000.5, MicroChem Corp., USA), and the dye was rhodamine B (RhB, J&K Scientific Ltd., Beijing, China). The gain media were the photoresist doped with the RhB dye in a ratio of 2 mg:1 mL and were mixed by a magnetic stirrer for 1 h before use. A thin active layer of the gain media was then deposited by a spin coater onto the silica microdisk. GOPTS (Aladdin, Shanghai, China) was mixed with ethanol in 1% volume ratio and utilized for the silanization of HD microdisk laser surfaces. The BSA (Merck Life Science, Shanghai, China) was diluted with PBS (Merck Life Science, Shanghai, China) to concentrations of 1, 10, and 100 ag mL^{-1}; 1, 10, and 100 fg mL^{-1}; 1, 10, and 100 pg mL^{-1}; and 1, 10, and 100 ng mL^{-1}. The goat anti-human IgG, human IgG, and horse IgG were obtained from Dingguo Changsheng Biotechnology (Beijing, China). The human IgG was diluted with PBS to concentrations of 1, 10, and 100 ag mL^{-1}; 1, 10, and 100 fg mL^{-1}; 1, 10, and 100 pg mL^{-1}; 1, 10, and 100 ng mL^{-1}; and 1, 10, and 100 μg mL^{-1}. The human IgA was purchased from BoYao Biotechnology (Shanghai, China). The experiments were carried in the commercial artificial serum purchased from InnoReagents (Huzhou, China). According to the supplier's specifications, the artificial serum was composed of water (> 95%), proprietary formulation with

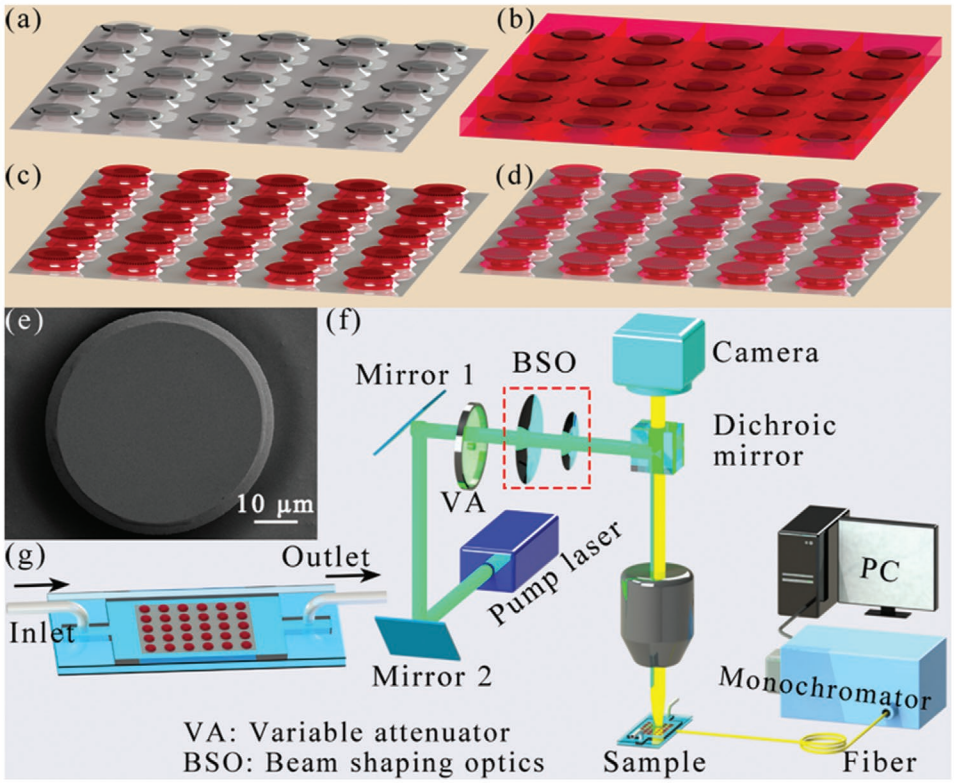

Figure 6. Fabrications of HD microdisk lasers and experimental setup. a) Schematic diagrams of a silica microdisk array. b) Gain media dripped on the silica microdisk array. c) After spin coating, the HD microdisk laser is fabricated. d) Magnetron sputtering of a SiO_2 layer to the surface of microdisk lasers. e) Top-view SEM image of the HD microdisk laser. f) Experimental setup schematic of the HD microdisk lasers. g) Schematic diagram of HD microdisk lasers combined with a microchannel.

nonhazardous components (4%), and 2-chloroacetamide (< 0.1%). The different concentrations of human IgG solutions, diluted in the artificial serum to simulate human bodily fluids, from 1 ag mL^{-1} to 100 μg mL^{-1} were increased by a factor of 10 for each successive solution.

Fabrication Processes: The fabrication process of the silica microdisks was similar to refs. [36,59–61] and the schematic diagram of the silica-microdisk array is shown in **Figure 6**a. The gain media were dripped onto the substrate of the microdisk, as shown in Figure 6b. After the spin-coating process, a thin active layer was coated on the surface of the silica microdisks, as shown in Figure 6c. After following with the exposure and curing processes, the HD microdisk-laser array was formed. Figure 6d presents a silica layer (≈40 nm in thickness) deposited on the surface of HD microdisk lasers by magnetron sputtering to avoid the biological functionalization directly on the surface of the photoresist (SU-8). The subsequent biological functionalization was conducted on the silica layer.[62] Figure 6e shows the top-view of the SEM images of the HD microdisk lasers whose diameter was ≈52.9 μm.

Experimental Setup: The experimental setup is shown in Figure 6f. The pump laser was a nanosecond pulse laser (532 nm, 10 Hz, Minilite II, Continuum Electro Optics, USA). A monochromator (Acton SpectraPro 2750, Princeton Instruments, USA) was employed to collect the laser spectra. The beam shaping optics were used to control the size of the pumped laser, and a variable attenuator was used to adjust the power of the pumped laser. The laser beam spot was coupled to the microscope system, and further focused to about 60 μm under a 10 × objective lens. The sample was moved to the laser spot using a 3D stage. The output laser of the HD microdisk was collected by an optical fiber bundle. The laser was then coupled to the monochromator and detected by the electron multiplier charge coupled device (DV401A, Andor iDus, UK). The spectral resolution of the spectrometer was about 0.015 nm. Figure 6g shows the HD microdisk-laser array combined with the microfluidic channel. The microfluidic channel is a device that combines a clean glass slide and a patterned polydimethylsiloxane (PDMS) leaf. The PDMS leaf was molded from a splicing glass mold and the manufacturing process could be referred to ref. [28]. A syringe pump was used to extract the solution into or out of the microfluidic channel to replace the solution. All the experiments were performed in an indoor environment (22 °C and 40% humidity). The simulations were conducted by using the commercial FEM software (COMSOL Multiphysics).

Supporting Information

Supporting Information is available from the Wiley Online Library or from the author.

Acknowledgements

Z.G. and Y.Q. contributed equally to this work. This work was financially supported by Special Project of National Key Technology R&D Program of the Ministry of Science and Technology of China (2016YFC0201401); National Natural Science Foundation of China (grant no. 61922040); Shanghai Science and Technology Committee Grant (18JC1411500); and National Key Basic Research Program of China (Program 973: 2015CB352006).

Conflict of Interest

The authors declare no conflict of interest.

Keywords

human IgG detection, label-free biosensors, microdisk lasers, optofluidics

Received: January 13, 2020
Revised: April 15, 2020
Published online:

[1] Q. J. Wang, C. Yan, N. Yu, J. Unterhinninghofen, J. Wiersig, C. Pflügl, L. Diehl, T. Edamura, M. Yamanishi, H. Kan, F. Capasso, *Proc. Natl. Acad. Sci. USA* **2010**, *107*, 22407.
[2] M. R. Foreman, J. D. Swaim, F. Vollmer, *Adv. Opt. Photonics* **2015**, *7*, 168.
[3] J. Ward, O. Benson, *Laser Photonics Rev.* **2011**, *5*, 553.
[4] A. Chiasera, Y. Dumeige, P. Féron, M. Ferrari, Y. Jestin, G. N. Conti, S. Pelli, S. Soria, G. Righini, *Laser Photonics Rev.* **2010**, *4*, 457.
[5] X. Zhang, L. Ren, X. Wu, H. Li, L. Liu, L. Xu, *Opt. Express* **2011**, *19*, 22242.
[6] X. Tu, X. Wu, M. Li, L. Liu, L. Xu, *Opt. Express* **2012**, *20*, 19996.
[7] Y. J. Chen, U. Schoeler, C. H. B. Huang, F. Vollmer, *Small* **2018**, *14*, 1703705.
[8] Y. Zhi, X. C. Yu, Q. Gong, L. Yang, Y. F. Xiao, *Adv. Mater.* **2017**, *29*, 1604920.
[9] J. Su, *Sensors* **2017**, *17*, 540.
[10] F. Vollmer, L. Yang, *Nanophotonics* **2012**, *1*, 267.
[11] S. Liu, W. Sun, Y. Wang, X. Yu, K. Xu, Y. Huang, S. Xiao, Q. Song, *Optica* **2018**, *5*, 612.
[12] E. Ozgur, K. E. Roberts, E. O. Ozgur, A. N. Gin, J. R. Bankhead, Z. Wang, J. Su, *Anal. Chem.* **2019**, *91*, 11872.
[13] Z. Guo, Q. Lu, C. Zhu, B. Wang, Y. Zhou, X. Wu, *Opt. Express* **2019**, *27*, 12424.
[14] X. Feng, G. Zhang, L. K. Chin, A. Q. Liu, B. Liedberg, *ACS Sens.* **2017**, *2*, 955.
[15] T. Reynolds, N. Riesen, A. Meldrum, X. Fan, J. M. Hall, T. M. Monro, A. François, *Laser Photonics Rev.* **2017**, *11*, 1600265.
[16] Y. Zhang, T. Zhou, B. Han, A. Zhang, Y. Zhao, *Nanoscale* **2018**, *10*, 13832.
[17] Z. Chen, M. Li, X. Wu, L. Liu, L. Xu, *Opt. Express* **2015**, *23*, 17659.
[18] Y. Zhang, H. Peng, X. Qian, Y. Zhang, G. An, Y. Zhao, *Sens. Actuators, B* **2017**, *244*, 393.
[19] J. Velázquez-Gonzálezab, D. Monzón-Hernándeza, D. Moreno-Hernándeza, F. Martínez-Piñónb, I. Hernández-Romano, *Sens. Actuators, B* **2017**, *242*, 912.
[20] T. Tang, X. Wu, L. Liu, L. Xu, *Appl. Opt.* **2016**, *55*, 395.
[21] S. Wondimu, M. Hippler, C. Hussal, A. Hofmann, S. Krämmer, J. Lahann, H. Kalt, W. Freude, C. Koos, *Opt. Express* **2018**, *26*, 3161.
[22] T. Reynolds, A. Franc¸ois, N. Riesen, M. E. Turvey, S. J. Nicholls, P. Hoffmann, T. M. Monro, *Anal. Chem.* **2016**, *88*, 4036.
[23] U. Bog, F. Brinkmann, S. F. Wondimu, T. Wienhold, S. Kraemmer, C. Koos, H. Kalt, M. Hirtz, H. Fuchs, S. Koeber, T. Mappes, *Adv. Sci.* **2015**, *2*, 1500066.
[24] T. Siegle, J. Kellerer, M. Bonenberger, S. Krmmer, C. Klusmann, M. Mller, H. Kalt, *Opt. Express* **2018**, *26*, 3579.
[25] Y. C. Chen, X. Tan, Q. Sun, Q. Chen, W. Wang, X. Fan, *Nat. Biomed. Eng.* **2017**, *1*, 724.
[26] H. Li, L. Shang, X. Tu, L. Liu, L. Xu, *J. Am. Chem. Soc.* **2009**, *131*, 16612.
[27] Z. Zhang, W. Morrish, K. Gardner, S. Yang, Y. Yang, A. Meldrum, *Opt. Express* **2019**, *27*, 26967.
[28] Z. Guo, H. Wang, C. Zhao, L. Chen, S. Liu, J. Hu, Y. Zhou, X. Wu, *Nanomaterials* **2019**, *9*, 1439.
[29] U. Bog, F. Brinkmann, H. Kalt, C. Koos, T. Mappes, M. Hirtz, H. Fuchs, S. Kber, *Small* **2014**, *10*, 3863.
[30] C. Gong, Y. Gong, X. Zhao, Y. Luo, Q. Chen, X. Tan, Y. Wu, X. Fan, G. D. Peng, Y. J. Rao, *Lab Chip* **2018**, *18*, 2741.
[31] M. de Goede, L. Chang, J. Mu, M. Dijkstra, R. Obregón, E. Martínez, L. Padilla, F. Mitjans, S. M. Garcia-Blanco, *Opt. Lett.* **2019**, *44*, 5937.
[32] G. S. Murugan, J. S. Wilkinson, M. N. Zervas, *Opt. Express* **2009**, *17*, 11916.
[33] N. Riesen, T. Reynolds, A. Franc¸ois, M. R. Henderson, T. M. Monro, *Opt. Express* **2015**, *23*, 28896.
[34] I. M. White, H. Oveys, X. Fan, *Opt. Lett.* **2006**, *31*, 1319.
[35] L. Zhao, Y. Wang, Y. Yuan, Y. Liu, S. Liu, W. Sun, J. Yang, H. Li, *Opt. Commun.* **2017**, *402*, 181.
[36] H. Lee, T. Chen, J. Li, K. Y. Yang, S. Jeon, O. Painter, K. J. Vahala, *Nat. Photonics* **2012**, *6*, 369.
[37] T. M. Aminabhavi, *J. Chem. Eng. Data* **1984**, *29*, 54.
[38] H. Zhu, I. M. White, J. D. Suter, P. S. Dale, X. Fan, *Opt. Express* **2007**, *15*, 9139.
[39] S. Arnold, M. Khoshsima, I. Teraoka, S. Holler, F. Vollmer, *Opt. Lett.* **2003**, *28*, 272.
[40] E. Melnik, R. Bruck, P. Müellner, T. Schlederer, R. Hainberger, M. Lämmerhofer, *J. Biophotonics* **2016**, *9*, 218.
[41] Z. Li, C. Zhu, Z. Guo, B. Wang, X. Wu, Y. Fei, *Micromachines* **2018**, *9*, 274.
[42] H. Ghali, P. Bianucci, Y. A. Peter, *Sens. Bio-Sens. Res.* **2017**, *13*, 9.
[43] H. M. Wong, J. J. Wang, C. H. Wang, *Ind. Eng. Chem. Res.* **2001**, *40*, 933.
[44] S. Dong, M. Tong, D. Zhang, T. Huang, *Sens. Actuators, B* **2017**, *251*, 650.
[45] Q. Wang, J. Y. Jing, B. T. Wang, *IEEE Trans. Instrum. Meas.* **2019**, *68*, 3350.
[46] M. Lu, H. Zhu, C. G. Bazuin, W. Peng, J. F. Masson, *ACS Sens.* **2019**, *4*, 613.
[47] L. Liang, L. Jin, Y. Ran, L. P. Sun, B. O. Guan, *Anal. Chem.* **2018**, *90*, 10851.
[48] M. de Goede, M. Dijkstra, R. Obregón, J. Ramón-Azcón, E. Martínez, L. Padilla, F. Mitjans, S. M. Garcia-Blanco, *Opt. Express* **2019**, *27*, 18508.
[49] A. J. Qavi, T. M. Mysz, R. C. Bailey, *Anal. Chem.* **2011**, *83*, 6827.
[50] O. Scheler, J. T. Kindt, A. J. Qavi, L. Kaplinski, B. Glynn, T. Barry, A. Kurg, R. C. Bailey, *Biosens. Bioelectron.* **2012**, *36*, 56.
[51] M. S. Luchansky, A. L. Washburn, M. S. McClellan, R. C. Bailey, *Lab Chip* **2011**, *11*, 2042.
[52] V. R. Dantham, S. Holler, C. Barbre, D. Keng, V. Kolchenko, S. Arnold, *Nano Lett.* **2013**, *13*, 3347.
[53] S. Berneschi, F. Baldini, A. Cosci, D. Farnesi, G. N. Conti, C. T. S. Tombelli, S. Pelli, A. Giannetti, *Sens. Actuators, B* **2017**, *242*, 1057.
[54] H. Wang, H. Wang, M. Zhang, Y. Jia, Z. Li, *RSC Adv.* **2019**, *9*, 32906.
[55] Y. Qian, T. Fan, Y. Yao, X. Shi, X. Liao, F. Zhou, F. Gao, *Sens. Actuators, B* **2018**, *254*, 483.
[56] S. F. Wondimu, S. von der Ecken, R. Ahrens, W. Freude, A. E. Guber, C. Koos, *Lab Chip* **2017**, *17*, 1740.
[57] X. Yang, Y. Luo, Y. Liu, C. Gong, Y. Wang, Y. J. Rao, G. D. Peng, Y. Gong, *Lab Chip* **2020**, *20*, 923.
[58] N. Sandhyarani, in *Electrochemical Biosensors*, (Ed: A. A. Ensafi), Elsevier, Amsterdam, Netherlands **2019**, Ch. 3.
[59] C. Zheng, X. Jiang, S. Hua, L. Chang, G. Li, H. Fan, M. Xiao, *Opt. Express* **2012**, *20*, 18319.
[60] G. Anetsberger, O. Arcizet, Q. P. Unterreithmeier, R. Rivière, A. Schliesser, E. M. Weig, J. P. Kotthaus, T. J. Kippenberg, *Nat. Phys.* **2009**, *5*, 909.
[61] G. Wang, M. Zhao, J. Ma, G. Li, Y. Chen, X. Jiang, M. Xiao, *Sci. China Math.* **2015**, *58*, 1.
[62] J. C. Ramirez, J. N. Schianti, D. E. Souto, L. T. Kubota, H. E. Hernandez-Figueroa, L. H. Gabrielli, *Biomed. Opt. Express* **2018**, *9*, 2168.

